Research Article

Novel Cocrystals of Glipizide: Green Supramolecular Mechanosynthesis

Dimpy Rani[1], Sarb Sukhmani Kaur Dargan[2], Parnika Goyal[2] and Renu Chadha[2]*

[1]G D Goenka University, Gurgaon-122103, India

[2]University Institute of Pharmaceutical Sciences, Panjab University, Chandigarh-160014, India

*Corresponding author: Renu Chadha, Department of Pharmaceutical Sciences, University Institute of Pharmaceutical Sciences, Panjab University, Chandigarh-160014, India.

Abstract

The present research demonstrates the five novel cocrystals of glipizide (GPZ) with picolinic acid (PA), adipic acid (AA), isonicotinic acid (INA), fumaric acid (FA) and sorbic acid (SRA). The cocrystals were prepared via green supramolecular mechanosynthesis approach and exhibited 1:1 stoichiometric ratio. The cocrystals were characterized by thermal (DSC) and spectroscopic (PXRD, FTIR and SSNMR) techniques. PXRD data was used to elucidate the crystal structure. GPZ-PA, GPZ-AA, GPZ-INA, GPZ-FA and GPZ-SRA were found to be crystallized in triclinic and monoclinic crystal systems, which exist in P-1, P1 and P21 space groups. Remarkable improvement in solubility and intrinsic dissolution rate (IDR) was observed along with significant reduction in rat blood serum glucose level and high C_{max} in comparison to GPZ.

Keywords: Glipizide; Cocrystals; Crystal structure; Solubility; Pharmacological studies

Abbreviations: GPZ: Glipizide; PA: Picolinic Acid; AA: Adipic Acid; INA: Isonicotinic Acid; FA: Fumaric Acid; SRA: Sorbic Acid; API: Active Pharmaceutical Ingredients; GRAS: Generally Regarded as Safe; LAG: Liquid Assisted Grinding; DSC: Differential Scanning Calorimeter; PXRD: Powder X-ray Diffraction; FTIR: Fourier Transform Infrared; SSNMR: Solid State Nuclear Magnetic Rasonance

Introduction

Drug development via the traditional synthetic methods involves the usage of a large quantity of chemicals which in turn generates by-products that adversely affect the environment [1]. In this case, it is the need of the hour to probe the environmentally friendly i.e., green alternative synthetic strategies, which are more selective and economical for the development and optimization of the existing APIs (Active Pharmaceutical Ingredients) at the industrial scale [2-4]. As compared to the solvent based chemical reactions, the solid-state reactions are the viable green approach to achieve these goals in an efficient manner. Solid state mechanochemistry is of great interest as it caters the opportunity to widen the scope of synthetic reactions and build up more sustainable methods. The other alluring aspects of these eco-friendly reactions include little or no use of solvents, high yield and purity of products, stochiometric and polymorphic control, cost effectiveness and time efficiency [3,5-7]. Mechanosynthesis has emerged as a versatile tool for the supramolecular synthesis in the pharmaceutical field. Modification in the intermolecular interactions leads to the variation in the crystal lattice, which can result in the improvement of physicochemical properties, and in

turn enhances the performances of pharmaceutical solids [8]. Based on these concepts, the manuscript has been emphasized to tailor supramolecular architecture by incorporating counter molecules in the lattice of API, leading to cocrystals. The use of GRAS (Generally Regarded as Safe) conformers, and acceptable solvents in nominal amount makes pharmaceutical cocrystallization technique as a part of green process. Out of various methods, liquid-assisted grinding (LAG) is preferable and commonly used method for the preparation of pharmaceutical cocrystals. The catalytic amount of solvent in the reactions enhances the molecular mobility and accelerates the reaction rate. Moreover, the addition of solvent also leads to generation of more crystalline products with control over polymorphic behavior [9-14]. The legal benefits and consideration as a new chemical entity of cocrystals also aids in making it a preferable choice to explore.

The present work is focused on the synthesis, characterization and evaluation of the cocrystals of glipizide (GPZ; Figure 1), an oral short-acting hypoglyceamic agent. GPZ is prescribed widely for treating type II diabetes and thus, grabs the attention to improve the clinical performance by ameliorating the setback of dissolution

limited solubility. There are diverse approaches that have been adopted to ameliorate the solubility of GPZ. These include solid dispersion, hydrotropy, micellar solubilization, nanoparticles, cyclodextrin complexes and co-inclusion complex formation [15-18]. The availability of numerous hydrogen bond donor and acceptor in GPZ and the ability of the cocrystals to customize the physicochemical properties at root level without forming or breaking the covalent bonds make the cocrystals a viable mean to enhance the solubility and the clinical performance of GPZ.
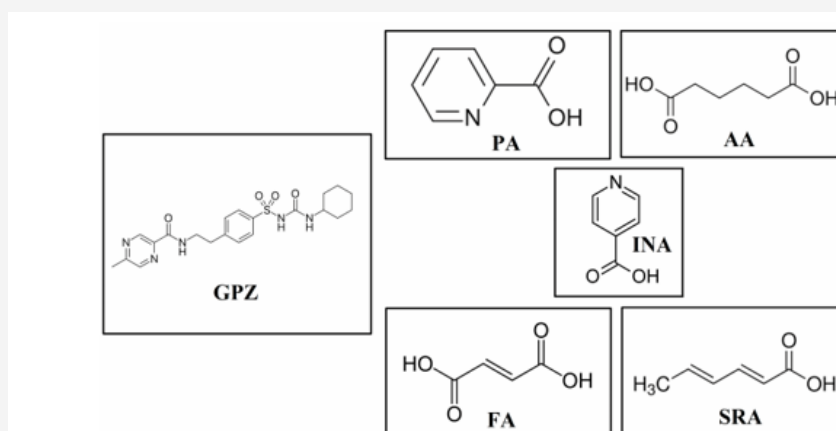
Figure 1: Chemical structure of GPZ and coformers.

As far as we are aware, not much work has been done on the cocrystallization of glipizide except one recent report in which authors have given four cocrystals of glipizide. However, they have not emphasized on their characterization as well as the structural parameters to identify hydrogen bonding in the crystal lattice which is vital for the stabilization of the cocrystals. In this manuscript, the isolation of pharmaceutically relevant cocrystals of glipizide (GRAS coformers: picolinic acid (PA), adipic acid (AA), isonicotinic acid (INA), fumaric acid (FA) and sorbic acid (SRA)) is described with focus on their proper characterization and structure elucidation (Figure 1).

Experimental

Materials

GPZ (≥99%) was obtained from La Pharma Pvt Ltd, Ludhiana, India, as a gift sample. All the chemicals and solvents were purchased from Sigma-Aldrich or E. Merck Ltd, and used as received.

Mechanosynthesis of cocrystal

Liquid assisted (solvent: ethanol) solid state grinding of the binary mixtures of GPZ with selected cocrystal formers (GPZ-PA (1:1; 44.55mg:12.31mg), GPZ-AA (1:1; 45.26mg:12.31mg), GPZ-INA (1:1; 45.26mg:12.31mg), GPZ-FA (1:1; 45.26mg:11.60mg), and GPZ-SRA (1:1; 45.26mg:11.21mg)) were performed. GPZ and different coformers, in their respective molar ratio were ground for 60 minutes in a mortar and pestle, with drop by drop addition of solvent simultaneously.

Differential Scanning Calorimetry (DSC)

DSC scans were recorded on Q 20 (TA-Instruments Inc., USA) with a refrigerated cooling system, at a heating rate of 10 °C/min under dry nitrogen purge (flow rate 50 ml/min). The samples were packed in aluminium pans and run for scan in the temperature range of 25-250 °C, using blank aluminium pan as reference.

Powder X-ray Diffraction (PXRD)

For the qualitative analysis of the cocrystals, PANalytical X'Pert Pro X-ray powder diffractometer (The Netherlands, Holland) with Cu source, at voltage of 40 kV and current 40 mA was used. The samples were scanned in the range of 5°-45° (2θ) with step size 0.02° θ/min, scan rate 3°/min and high resolution.

Fourier Transform Infrared (FTIR) spectroscopy

The samples were dispersed in potassium bromide and the pellet was prepared. The spectra of the pellets were collected using spectrum two IR spectrometer (Perkin Elmer, England). Each spectrum was derived from 4 accumulative scans in the range of 400-4000 cm^{-1} at a spectral resolution of 4 cm^{-1}.

Crystal structure determination from PXRD

The determination of the crystal structures of all the cocrystals was done by Material studio (BIOVIA 7.0) software using PXRD. The PXRD were obtained from PANalytical X'Pert Pro X-ray powder diffractometer (The Netherlands, Holland). The PXRD patterns were obtained in the range of 5°-45° (2θ) with step size 0.02 °θ/min, scan rate 3°/min and with 3250 reflections. These PXRDs were used to determine the crystal structures of the cocrystals. The process of analyzing the cell parameters consisted of four main steps: Indexing along with pawley refinement, structure solution, and reitveld refinement. Indexing is the crucial step in the structure determination, so the PXRD was pretreated by subtracting the background and smoothing followed by stripping. Diffraction peaks were searched in the range of 5°-40° 2θ and indexing was performed by X-CELL method, followed by pawley refinement, which generated the unit cell. Powder solve was performed on the unit cell with geometrically optimized GPZ and coformers. The chemical structures were optimized by DMol3 and simulated annealing algorithm in powder solve was used to adjust the position, orientation and the conformation of the structures in unit

Page 2 of 13

cell. Afterwards, reitveld refinement was done to get best possible crystal structure with least difference between experimental and calculated powder diffraction pattern.

Solid-state NMR (SSNMR) spectroscopy

Solid-state ^{13}C NMR spectra were obtained from Jeol-ECX 400 MHz spectrometer, operating at resonant frequency of 100 MHz. The data was collected at 273 K to minimize frictional heating effects. The spectra were referenced to methylene carbon of glycine (δglycine = 43.3 ppm) and then chemical shifts were recalculated to TMS. The other acquisition parameters for ^{13}CPMAS were: contact time, 3.5 ms; acquisition time, 29.0 ms; and relaxation delay, 5s.

Equilibrium solubility studies

The equilibrium solubility studies were performed by the method reported by Higuchi and conners [19] i.e., shake flask method. Excess amount of GPZ and its cocrystals were agitated for 24 hours at 200 rpm in a vial containing 5 ml of phosphate buffer (pH 7.4) using water bath shaker MSW-275 Macroscientific works, Delhi at 37 °C. The samples were filtered through 0.45μm membrane filter and quantified by HPLC.

Intrinsic dissolution studies (IDR)

IDR studies were performed using rotating disk dissolution test apparatus, DS 8000 (Lab India Analyticals) in phosphate buffer (pH 7.4) for 4 hours. The powder of GPZ and cocrystals (equivalent to 150 mg GPZ) was compressed to a 0.5 cm^2 disk with hydraulic press. The disk was placed in 500 ml phosphate buffer (pH 7.4), preheated at 37°C and rotated at 150 rpm. The samples were withdrawn (5 ml) manually at different intervals of time and the quantity of buffer in jar was maintained by adding fresh buffer equal to withdrawn quantity, filtered through 0.45μm membrane filter and quantified by HPLC.
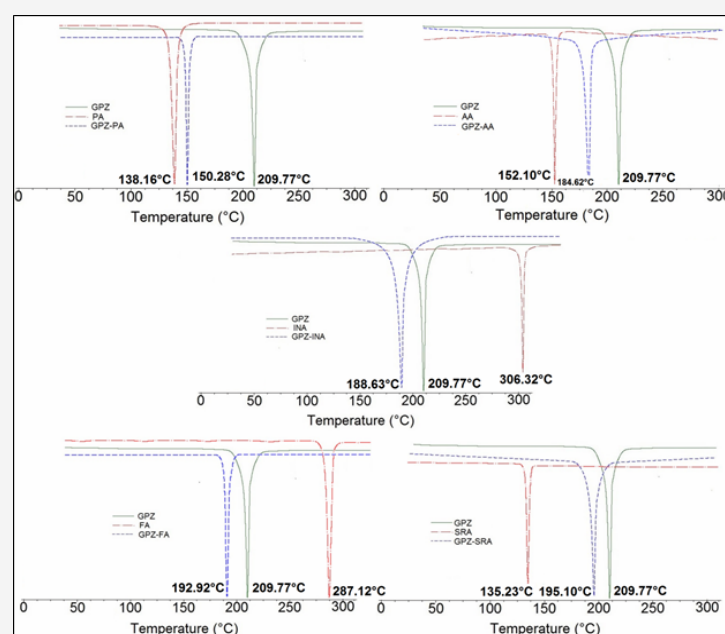
In Vivo studies

The pharmacodynamic and pharmacokinetic studies of GPZ and its cocrystals were performed on diabetic rats (male wistar rats; 3-4-week-old; 150-200 g). Streptozotocin with nicotinamide solution (45 mg/kg; prepared in citrate buffer (0.1 M) of pH 4.4) was injected via intraperitoneal route and the rats were diabetic after 48 hours [20]. GPZ and cocrystals equivalent to GPZ dose (5 mg/kg, suspended in 2% sodium CMC [21]) administered orally to the rats. The extent of reduction in blood glucose was measured at different intervals of time (0, 0.5, 1, 2, 3, 4, 5, 6 and 8 hrs). An enzymatic GOD – POD (glucose oxidase peroxidase) method [22] was used to analyze the concentration of glucose in blood. For the pharmacokinetic study, the blood samples from diabetic rats were withdrawn at different intervals of time for 8 hours. The plasma samples were quantified by HPLC and the pharmacokinetic parameters were calculated using PKSolver: An Add–in program [23], based on the linear trapezoidal method.

In both studies, the blood samples were withdrawn from retrobulbar venous plexus and the results were expressed in percentage mean ± SEM. The obtained data were compared statistically with control groups by Student's t test with $p < 0.05$ as the level of significance, using GraphPad Prism 6.0 software.
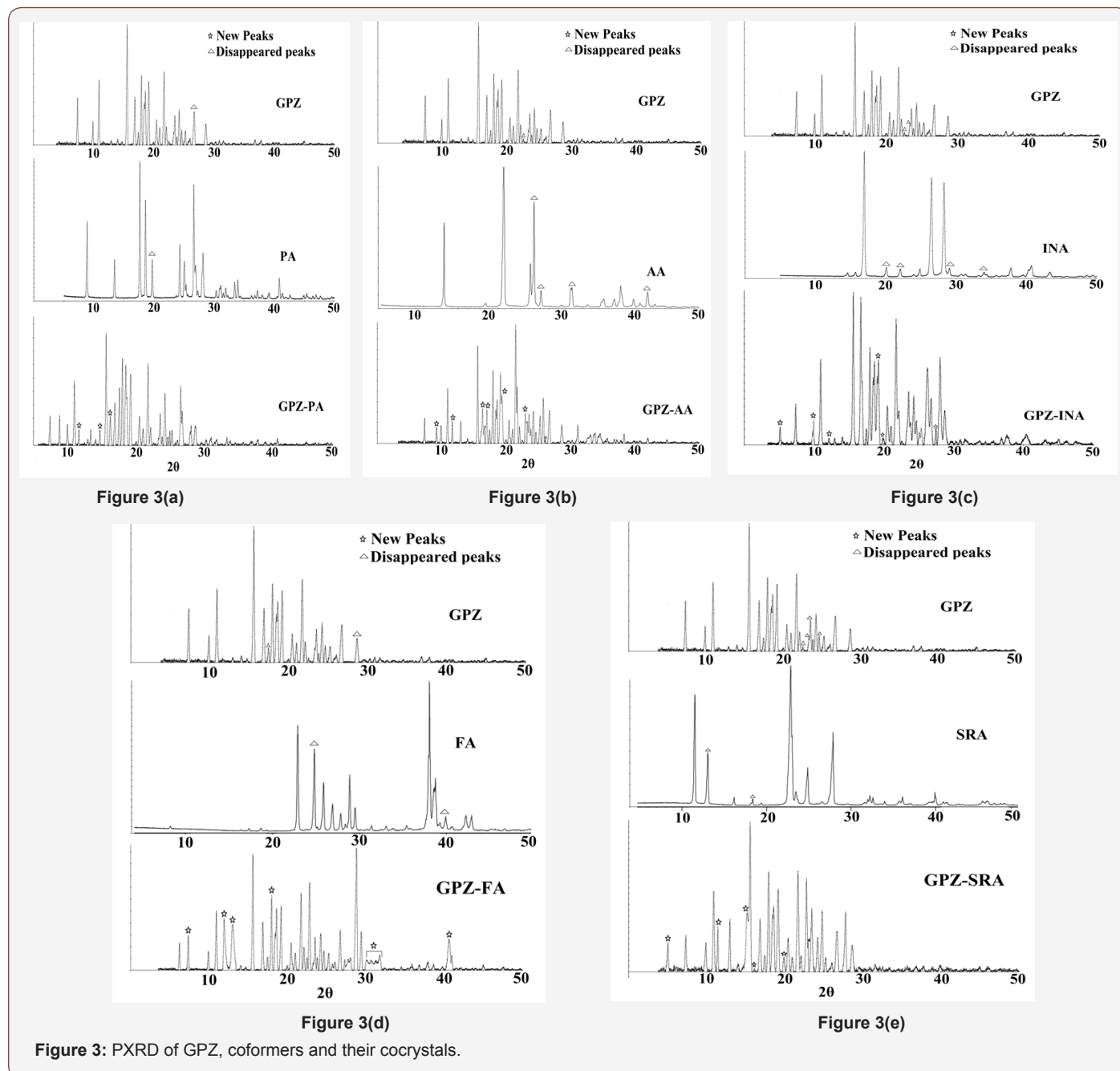
HPLC method

HPLC (Waters; Photodiode Array Detector) and Thermofisher C_{18} column (4.6 mm × 250 mm × 5 μm) were used to quantify the GPZ concentration using calibration plot. The samples (injection volume 10 μl) were eluted with isocratic mobile phase containing a mixture of acetonitrile: water (50:50) of pH 3 (pH was adjusted with orthophosphoric acid) in 10 minutes with flow rate 0.8 ml/min. GPZ peak was detected at 227 nm with retention time 6.6 min.

Results and Discussion

DSC

Figure 2: DSC thermograms of GPZ, coformers and cocrystals.

DSC thermograms (Figure 2) of the prepared solid forms namely GPZ-PA, GPZ-AA, GPZ-INA, GPZ-FA and GPZ-SRA showed a single melting endotherm at 150.28 °C, 184.62 °C, 188.63 °C, 192.92 °C and 195.10°C, respectively. These melting peaks are sharp and different from the GPZ (209.77°C) and respective coformers (PA-138.16°C; AA-152.10°C; INA-306.32°C; FA-287.12°C; SRA-135.23°C). The melting peak of GPZ-PA, GPZ-AA and GPZ-SRA is positioned between the endotherms of GPZ and corresponding coformers, which indicates the likelihood of cocrystal formation. In contrast to these, the endothermic peak of GPZ-INA and GPZ-FA appears before the melting peaks of GPZ and their respective coformers, which suggest the synthesis of either cocrystal or eutectic. However, the

DSC of the physical mixtures (given in supporting data; Figure S1) of all the crystalline phases in stoichiometric ratio 1:1 show the two broad peaks, representative of individual components. This corroborates the formation of cocrystals and at the same time negates the eutectic formation in GPZ-INA and GPZ-FA (Figure 2).

PXRD

The peaks in the PXRD patterns are the reflections from the atomic planes [24] in the crystal lattice and are the fingerprint for any crystalline material. The PXRD pattern of the obtained solid forms is unique and different from their parent components (Figure 3), indicating the generation of a new crystalline phase.

Figure 3(a)

Figure 3(b)

Figure 3(c)

Figure 3(d)

Figure 3(e)

Figure 3: PXRD of GPZ, coformers and their cocrystals.

GPZ-PA witness the appearance of many new peaks at 11.49°, 14.81°, 16.21° along with the disappearance of characteristic peaks of GPZ (26.74°) and PA (19.09°). Besides this, few peaks of GPZ at 17.44° and 24.24° merged with peaks of PA at 17.61° and 24.22°

respectively, to give a single and broad peak correspondingly at 17.56° and 24.20°. Moreover, the peaks of GPZ, positioned at 18.41° and 18.62° merged with peak of PA at 18.53° to give a split peak at 18.49° and 18.67°.

In GPZ-AA, new peaks at 10.10°, 11.62°, 16.20°, 16.46°, 16.84°, 19.35°, 22.80° and 26.30° were observed. The peaks at 22.52° of GPZ, at 26.08°, 27.07°, 31.52° and 42.26° of AA have disappeared. Apart from it, the peak of GPZ at 21.74° merged with 21.76°, a peak of AA, to give a broad and single peak at 21.75° in GPZ-AA.

Some new peaks, in GPZ-INA, at 5.03°, 10.03°, 11.72°, 18.83°, 19.83° and 27.65° appeared while some characteristic peaks at 22.52° and 23.27° of GPZ and at 20.12°, 22.09°, 29.06°, 34.02° of INA have disappeared.

In GPZ-FA, a few new peaks at 8.55°, 11.97°, 12.71°, 18.37°, 30.69°, 31.20°, 31.91°, 32.30° and 41.87° appeared, accompanied with disappearance of some of the peaks of GPZ at 17.44°, 28.60° and of FA, at 24.80°, 39.93°.

In GPZ-SRA, new peaks were observed at 5.32°, 11.19°, 15.30°, 19.50°, 22.96° while some characteristic peaks at 22.52°, 23.27°, 23.51°, 23.77°, 24.64° of GPZ and at 13.00°, 18.31° of SRA have disappeared. A few nearby peaks of GPZ and SRA merged to give either a new peak or a broad peak.

Besides these changes, many characteristics peaks of both GPZ and respective coformers, shifted significantly from their positions. All these noticeable changes in the PXRD are the indicator of the generation of new crystalline phases (Figure 3).

FTIR

FTIR spectra help to investigate the vibrational changes in the functional groups during supramolecular synthesis. In the cocrystals of GPZ, the significant changes have been seen in the sulfonylurea and amide group of GPZ and carboxylic acid groups of coformers. The changes in the wavenumber of different involved groups have been given in supporting information in Table S1 and FTIR spectra are given in Figure S2. The absence of any new peak in the region of 1650 cm^{-1} to 1550 cm^{-1}, negates the likelihood of proton transfer during cocrystallization. The variations in the position of characteristic peaks are indicative of some interactions between GPZ and coformers.

## Crystal structure determination from PXRD

The importance of the crystal structure determination can be marked as the physicochemical properties of the compounds are the outcome of the packing of the molecules and the interactions among them. As the crystallization of the ground powder could not yield the suitable crystals for single crystal analysis. So, the crystal structure was determined using the PXRD pattern. The pictures for the crystallized powders are given in (Figure 4).
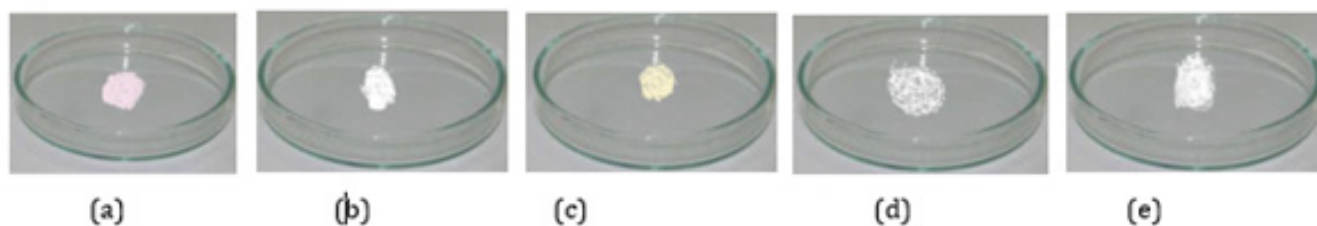
Figure 4: Pictures of the obtained crystallized cocrystals (a) GPZ-PA (b) GPZ-AA (c) GPZ-INA (d) GPZ-FA (e) GPZ-SRA.
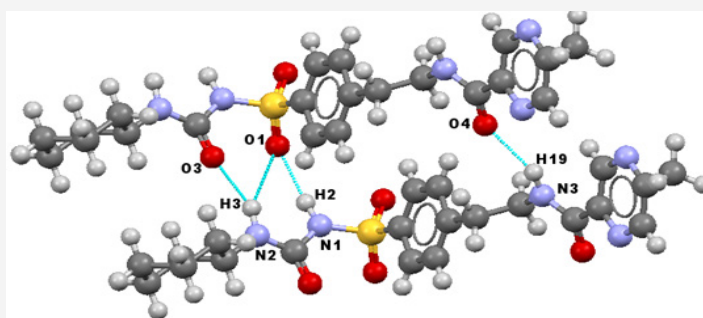
Figure 5 (a)
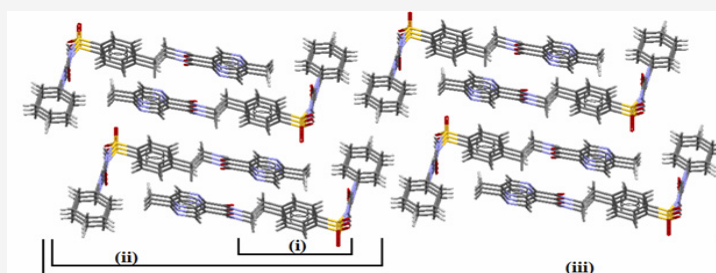
Figure 5 (b)

Figure 5: (a) Homomeric interactions in GPZ (b) arrangements of GPZ molecules in crystal lattice along a* axis; i) hydrogen bonded parallel GPZ molecules in chains, ii) interlocked pair, iii) layers linked via van der Waals forces (CCDC No: 292334 and 1516974, Refcode: SAXFED and SAXFED01) [21-22].

The crystal structure of GPZ is first reported by Burley [25] using PXRD and recently corroborated by Samie et al. [26] group using the single crystal x-ray diffraction. GPZ crystallizes in triclinic crystal system with P-1 space group. The hydrogen atom of one –NH$_{sulfonamide\ (sulfonylurea)}$ of GPZ interacts with oxygen atom of –SO$_{2sulfonylurea}$ of another GPZ, which forms N1–H2···O1 homosynthon [. Another –NH$_{amide\ (sulfonylurea)}$ of GPZ forms bifurcated hydrogen bonding with oxygen atom of –CO$_{sulfonylurea}$ and oxygen atom of –SO$_{2sulfonylurea}$ and generates N2–H3···O3 and N2–H3···O1 synthons. Besides this, -NH$_{amide}$ of GPZ is hydrogen bonded to oxygen of –CO$_{amide}$ of another GPZ molecule and forms N3–H19···O4 synthon (Figure 5a). The molecules of GPZ are sustained by 1D infinite chained pattern. These chains are packed in pairs, in an interlocking pattern and form layers, which are further linked to other layers *via* weak van der Waals forces (Figure 5b).

The insertion of the coformers in the crystal lattice of GPZ replaces the GPZ-GPZ interactions with GPZ-coformer interactions, resulting in the generation of cocrystals. GPZ-PA crystallizes in triclinic crystal system with P-1 space group, consisting one molecule of GPZ and one molecule of PA in asymmetric unit cell. The formation of cocrystal disrupts the already present homomeric N–H···O interactions in GPZ and establishes N–H···N and O–H···O type interactions in the crystal lattice of GPZ-PA. A new heterosynthon (O5–H28···O3; []) has formed between the oxygen atom of –CO$_{sulfonylurea}$ of GPZ and hydrogen atom of –OH$_{carboxylic}$ of PA. The –NH$_{sulfonamide\ (sulfonylurea)}$ of GPZ forms a new homodimer (N1–H2···N5) with N$_{ring}$ of another GPZ molecule, by breaking the previous N1–H2···O1 homosynthon. The GPZ molecules of two asymmetric units are sustained by ring motif. Besides this, the other –NH$_{amide\ (sulfonylurea)}$, which was involved in the homosynthon of GPZ, is now participating in the intramolecular bonding (N2–H3···O1; []) in the GPZ-PA (Figure 6a). In the crystal lattice of cocrystal, the repetitive entity of two bonded asymmetric units, stabilized *via* van der Waals forces (can be viewed along c-axis), forms the three-dimensional network of the crystal lattice (Figure 6b).
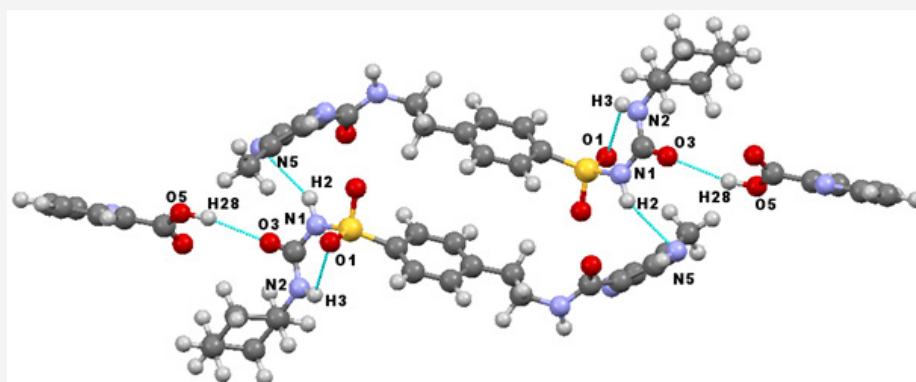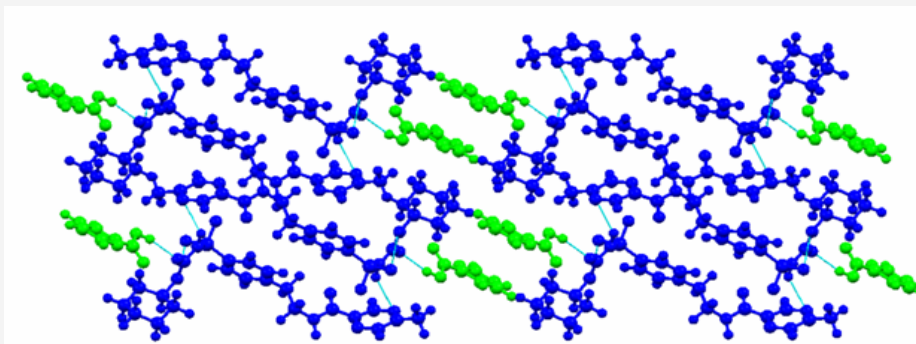

Figure 6(a)

Figure 6(b)

Figure 6: Crystal structure of GPZ-PA: (a) hydrogen bonding in GPZ and PA, (b) 2D view of the arrangement of GPZ and PA molecules along c-axis; GPZ and PA are represented by blue and green color respectively.

GPZ-AA also crystallizes in a triclinic crystal system with P-1 space group. The asymmetric unit encloses one molecule of GPZ and one molecule of AA. In the crystal structure of the cocrystal, –NH$_{amide\ (sulfonylurea)}$ of GPZ forms a new heterosynthon (N2–H3···O6; []) with oxygen of –CO$_{carboxylic}$ of AA, which has replaced N2–H3···O3 and N2–H3···O1 homosynthon in pure GPZ. Two more heterosynthons are formed between N$_{ring}$ of GPZ and hydrogen atoms of both –OH$_{carboxylic}$ of AA (O8–H37···N5; [and O5–H28···N4; []). Besides this, GPZ molecules are attached through a single point homosynthon (N3–H19···O3; []) which is formed between hydrogen atom of –NH$_{amide}$ and oxygen atom of –CO$_{amide}$ of two different GPZ molecules (Figure 7a) and was absent in the crystal lattice of pure GPZ. The crystal structure reveals that GPZ molecules are present in the folded 'hook' shaped conformations in the crystal lattice and are arranged in such a manner that the hook of two molecules faces each other. This leads to the interactions, forming the infinite chain (along c-axis). The AA molecules seem to be fitted in the cavities formed by aromatic rings of alternate GPZ molecules (Figure 7b & c).
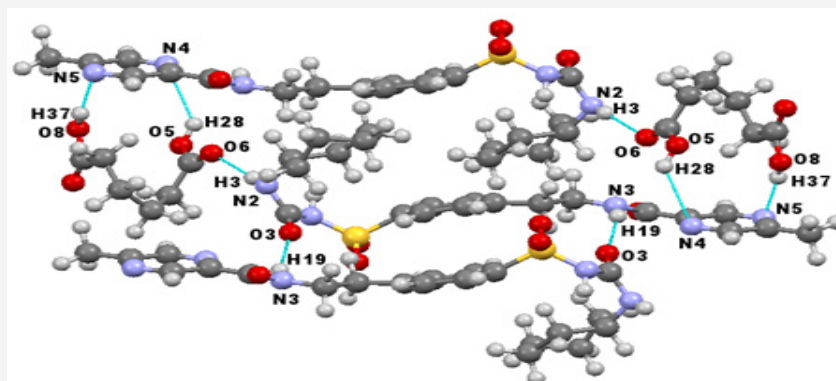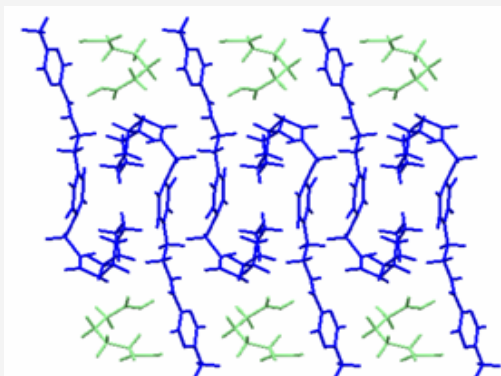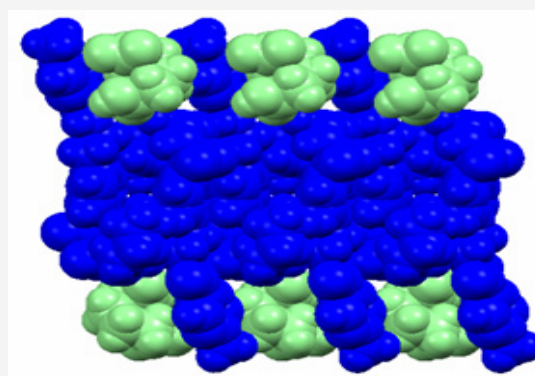
Figure 7(a)

Figure 7(b)

Figure 7(b)

Figure 7: Crystal structure of GPZ-AA: (a) hydrogen bonding between GPZ and AA, (b) 2D packing view of GPZ and AA molecules along c-axis, (c) 3D crystal structure of GPZ-AA in space fill mode; GPZ and AA are represented by blue and green color respectively.
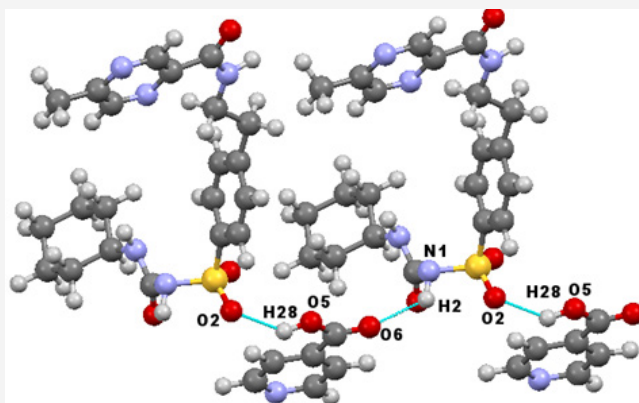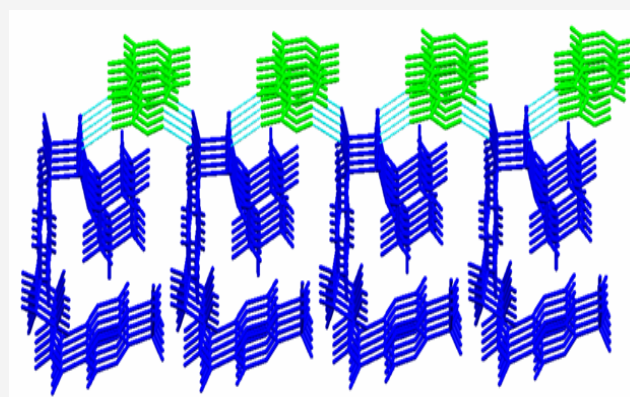

Figure 8 (a)
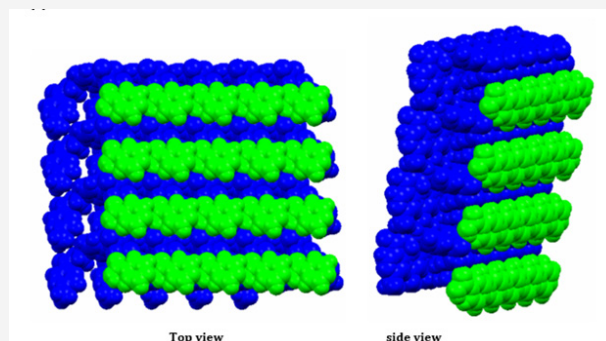

Figure 8 (b)

Figure 8 (c)

Figure 8: Crystal structure of GPZ-INA: (a) hydrogen bonding between GPZ and INA, (b) 2D packing view of GPZ and FA molecules along c*-axis, (c) the top and side view of 3D crystal structure of GPZ-INA in space fill mode; GPZ and INA are represented by blue and green color respectively.

The crystal structure of GPZ-INA reveals that it crystallizes in triclinic system (P1 space group), contains one molecule of GPZ and one molecule of INA in asymmetric unit. Two new heterosynthon N1–H2···O6 [and O5–H28···O1 [are formed by disrupting N1–H2···O1 homosyntyhon. One of the heterosynthon, N1–H2···O6 is formed between –NH$_{sulfonamide (sulfonylurea)}$ of GPZ and oxygen of –CO$_{carboxylic}$ of INA. The other one, O5–H28···O1 is formed by the hydrogen bonding between oxygen of –SO$_{2sulfonylurea}$ of GPZ and hydrogen of –OH$_{carboxylic}$ of INA (Figure 8a). In the crystal lattice, GPZ molecule exists in folded conformation and is connected to another GPZ molecule through a bridge of INA molecule. Both molecules are arranged alternatively and form an infinite chain. These chains are stacked over one another and attached through van der Waals forces (along c*-axis). In the space fill mode of three-dimensional supramolecular networks INA molecules seems to be entangled in the grooves formed by GPZ molecules (Figure 8b & c).

GPZ-FA belongs to the P-1 space group of triclinic crystal system and contains one molecule of GPZ and one molecule of FA in an asymmetric unit. In the presence of FA, all the preexisting homosynthons in GPZ were replaced by new homo and heterosynthons in the crystal lattice of GPZ-FA. A new one-point heterosynthon is formed between N$_{ring}$ of GPZ and hydrogen atom of –OH$_{carboxylic}$ of FA (O8–H31···N4; []). One molecule of GPZ is attached to another GPZ molecule through N3–H19···O3; [synthon (formed between hydrogen of –NH$_{amide}$ and oxygen of –CO$_{sulfonylurea}$). Besides this, one molecule of FA is connected to another FA molecule via O5–H28···O6; [synthon (formed between hydrogen of –OH$_{carboxylic}$ and oxygen of –CO$_{carboxylic}$) (Figure 9a). In the crystal lattice, the molecules are arranged in an infinite chained wavy pattern along c-axis, in such a way that a pair of GPZ molecule is bridged by a pair of FA molecules (Figure 9b & c).

Figure 9 (a)

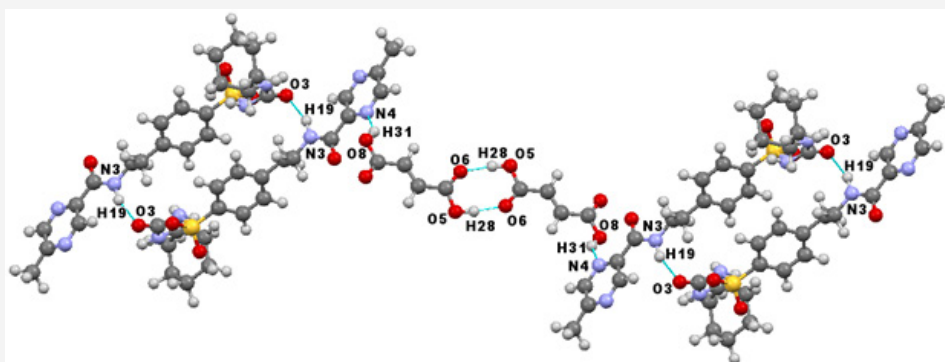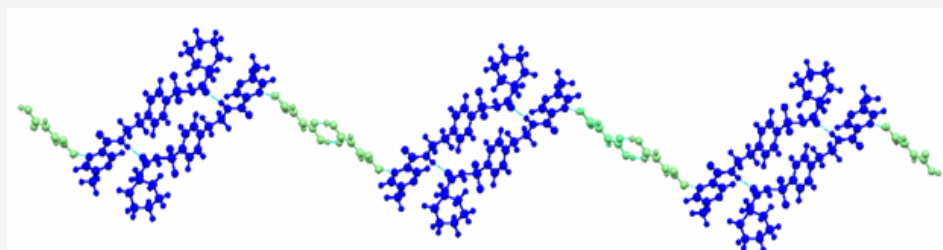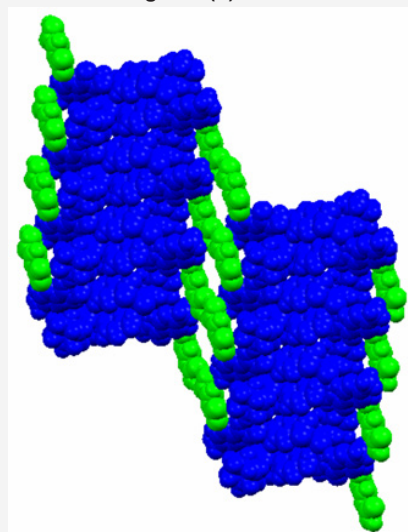**Figure 9(b)**

Figure 9(c)

Figure 9: Crystal structure of GPZ-FA: (a) hydrogen bonding between GPZ and FA, (b) 2D packing view of GPZ and FA molecules along c-axis, (c) 3D crystal structure of GPZ-FA in space fill mode along c-axis; GPZ and FA are represented by blue and green color respectively.

GPZ-SRA was found to exist in monoclinic crystal system with P21 space group and consist of one molecule of GPZ and one molecule of SRA in asymmetric unit cell. The inclusion of SRA in the crystal lattice of GPZ resulted in the breaking of all the preexisting homosynthons and generated new heterosynthons in GPZ-SRA (Figure 10a). One heterosynthon N2–H3···O6 [is formed between the hydrogen atom of –NH$_{amide (sulfonylurea)}$ of GPZ and oxygen atom of –CO$_{carboxylic}$ of SRA. The oxygen atom of –SO$_{2sulfonylurea}$ (O1) of GPZ, which was occupied in the formation of N1–H2···O1 homosynthon in pure

GPZ, is now hydrogen bonded to hydrogen atom of –OH$_{carboxylic}$ of SRA to give a heterosynthon O5–H28···O1 [. In the crystal lattice, GPZ and SRA molecules are arranged alternatively and sustained by chained synthons. These chains are linked to each other in a parallel manner by van der Waals forces. Upon viewing along b-axis, GPZ molecules seem to be present in dimers, embedded with SRA molecules and these layers constitute the supramolecular network of cocrystal (Figure 10b & c).
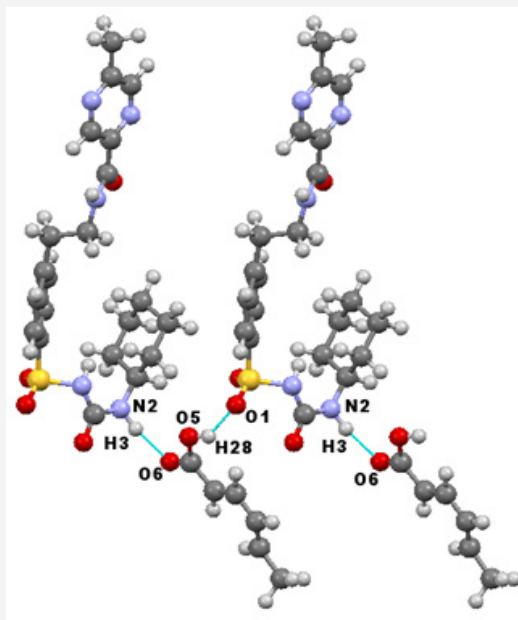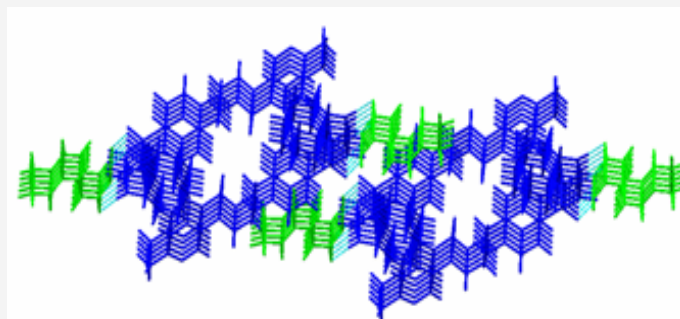

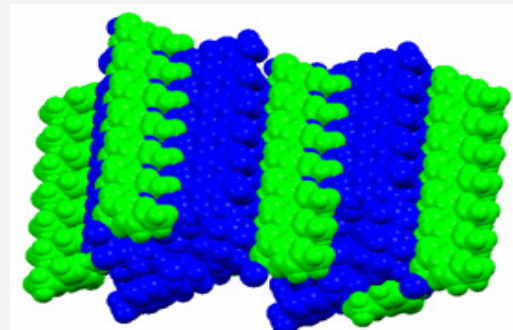**Figure 10 (a)**

Figure 10 (b)

Figure 10 (c)

Figure 10: Crystal structure of GPZ-SRA: (a) the angular displacement of the planes of GPZ and SRA in an asymmetric unit, (b) 2D packing view of GPZ and SRA molecules along b-axis, (c) 3D layers in crystal structure of GPZ-SRA in space fill mode; GPZ and SRA are represented by blue and green color respectively.

Table 1: Crystallographic parameters of cocrystals of GPZ.

Parameters	GPZ-PA	GPZ-AA	GPZ-INA	GPZ-FA	GPZ-SRA
Chemical formula	$C_{21}H_{27}N_5O_4S$; $C_6H_5NO_2$	$C_{21}H_{27}N_5O_4S$; $C_6H_{10}O_4$	$C_{21}H_{27}N_5O_4S$; $C_6H_5NO_2$	$C_{21}H_{27}N_5O_4S$; $C_4H_4O_4$	$C_{21}H_{27}N_5O_4S$; $C_6H_8O_2$
Stoichiometry	1:01	1:01	1:01	1:01	1:01
Temperature	Room temperature as specified 25°C	Room temperature as specified 25°C	Room temperature as specified 25°C	Room temperature as specified 25°C	Room temperature as specified 25°C
Crystal system	Triclinic	Triclinic	Triclinic	Triclinic	Monoclinic
Space group	P-1	P-1	P1	P-1	P21
a (Å)	24.0864	24.3818	24.3602	25.6521	16.6812
b (Å)	8.988	9.2343	9.0222	9.6856	8.055

Page 9 of 13

c (Å)	6.888	5.6605	6.7457	5.488	23.0561
α (deg)	82.02	77.92	90.36	78.56	90
β (deg)	91.78	93.59	93.58	93.4	105.07
γ (deg)	96.37	96.66	95.97	96.53	90
Z	2	2	2	2	2
Vol. (Å3)	1467.42	1236.87	1471.52	1326.8	2991.39
2θ range	5°-45°	5°-45°	5°-45°	5°-45°	5°-45°
Rwp	7.62	7.8	8.52	8.06	9.25
CCDC No	1555857	1555858	1555859	1555860	1555863

The crystallographic parameters of the cocrystals are summarized in Table 1 whereas the geometrical parameters are given in Table S2. The rietveld fit profile (comparison of simulated and experimental PXRD pattern) has been given in the supporting information (Figure S3). The obtained Rwp values for all the cocrystals are in the acceptable range (Table 1).

SSNMR

The formation of cocrystals *i.e.*, new crystalline phase is always coupled with change in chemical environment, which arises due to the changes in the interactions between drug and coformers.

The solid state ^{13}C NMR along with crystal structure provides the irrefutable evidence of hydrogen bonding, leading to the cocrystal formation, particularly in cases where single crystals are difficult to isolate.

The solid state ^{13}C NMR spectra of cocrystals of GPZ (Figure 11), in comparison to GPZ and respective coformers also supported the crystal structures, determined from PXRD pattern. The significant changes are observed in the neighboring carbon atoms of nitrogen and oxygen atoms. The note worthy changes is observed in the ^{13}C chemical shift of C2, C3, C4, C14, C15, C16, C17, C18 and C20 of GPZ and C22 of coformers (Table 2).

Table 2: ^{13}C Chemical shift of GPZ and its cocrystals.

Carbon Number	GPZ	GPZ-PA	GPZ-AA	GPZ-INA	GPZ-FA	GPZ-SRA
C2	137	136.86	136.68	136.91	136.71	137.37
C3	159.32	158.95	159.74	158.9	159.58	159.03
C4	51.12	51.43	51.47	51.39	51.38	51.38
C14	42.32	42.59	42.57	42.6	42.5	42.5
C15	166.06	165.5	165.57	165.48	165.39	165.37
C16	142.98	143.16	143.2	142.74	143.13	143.16
C17	144.78	145.01	144.96	144.97	144.99	144.69
C18	151.27	151.5	151.46	151.04	151.4	151.36
C20	143.83	144.04	144.06	143.07	143.64	143.68
C22		166.18	181.66	166.34	172.07	173.59
		(166.50 in PA)	(182.12 in AA)	(166.83 in INA)	(172.89 in FA)	(174.18 in SRA)

In GPZ-PA, the peak corresponding to C2 (attached to S1 atom) shifted upfield, which supports the involvement of O1 (attached to S1 atom) in the formation of new intramolecular hydrogen bond, N2–H3···O1 (r (H···A): 2.712 Å) by replacing intermolecular N2–H3···O1 (r (H···A): 2.592 Å) hydrogen bond. The upfield shifting of C3 (attached to O3) is indicative of formation of O5–H28···O3 (r (H···A): 2.400 Å) hydrogen bond by replacing N2–H3···O3 (r (H···A): 2.196 Å) hydrogen bond. Moreover, the downfield shift was observed in C4 (attached to N2), which may be due to the no longer availability of H3 as bifurcated hydrogen donor. Similarly, the downfield shifting of C14 (attached to N3) and upfield shifting of C15 (attached to O4) confirm the breaking of N3–H19···O4 homosynthon. Besides this, the downfield shifting of both C18 and C20 (attached to N5) also corroborate the formation of N1–H2···N5 heterosynthon.

The upfield and downfield shifting of C2 (attached to S1) and C3 (attached to O3) respectively, in GPZ-AA, confirm the breaking of N1–H2···O1 synthon. The downfield shifting of C14 (attached to

N3) along with upfield shifting of C15 (attached to O4) substantiate the formation of a N3–H19···O3 (r (H···A): 1.893 Å) hydrogen bond by replacing N3–H19···O4 (r (H···A): 2.231 Å) hydrogen bond and non availability of O4 as an acceptor. The downfield shifting of C4 (attached to N2) may be due to the disappearance of bifurcated hydrogen bonding by H3 in the cocrystal and formation of N2–H3···O6 synthon (r (H···A): 2.056 Å), in place of N2–H3···O1 (r (H···A): 2.592 Å) synthon. Besides this, the downfield shifting of C16, C17, C18, C20 (attached to N4 and N5) and upfield shifting of C22 and C27 (attached to O5, O6, O7 and O8 of AA) shows the presence of O8–H37···N5 and O5–H28···N4 heterosynthon along with the non-availability of O7 as an acceptor.

In GPZ-INA, the upfield shifting of C2 (attached to S1), C3 (attached to O3) and downfield shifting of C4 (attached to N2) gives an idea of breaking of N1–H2···O1/N2–H3···O1 and N2–H3···O3 hydrogen bonds. The marginal shifting of C2 also indicates the simultaneous involvement of O1 in the formation of another hydrogen bond i.e., O5–H28···O6. The downfield shifting of C14

(attached to N3) along with upfield shifting of C15 (attached to O4), suggests the breaking of N3–H19⋯O4 homosynthon. The upfield shifting of C22 (attached to O5 and O6) indicates the perturbation in the already present hydrogen bonded network in cofomer and supports the formation of N1–H2⋯O6 heterosynthon.

Cocrystal GPZ-FA shows the upfield shifting of C2 (attached to S1) and downfield shifting of C3 (attached to O3) and C4 (attached to N2) suggests the breaking of N1–H2⋯O1/N2–H3⋯O1 and N2–H3⋯O3 homosynthons. The downfield shifting of C14 (attached

to N3) and upfield shifting of C15 (attached to O4) indicates the breaking of N3–H19⋯O4 hydrogen bond. The downfield shifting of C3 (attached to O3) and C14 (attached to N3) also confirm the participation of O3 and N3–H19 in the formation of another hydrogen bond N3–H19⋯O3 r (H⋯A): 1.872 Å) in comparison N2–H3⋯O3 r (H⋯A): 2.196 Å) homosynthon. The upfield shifting of C22 and C25 (attached to O5, O6, O7 and O8) and marginal downfield shifing of C16 and C17 (attached to N4) confirm the presence of O8–H31⋯N4 synthon.
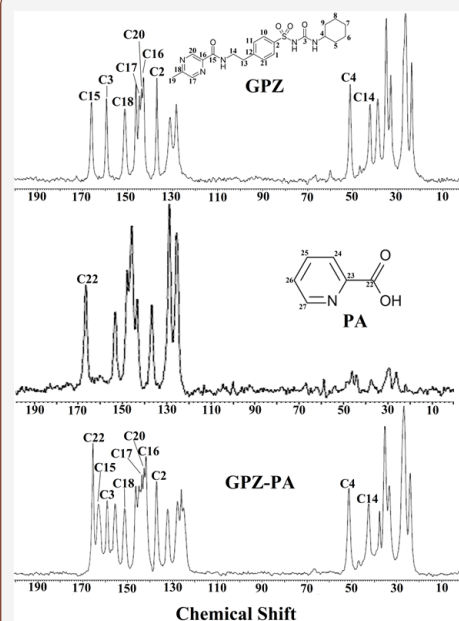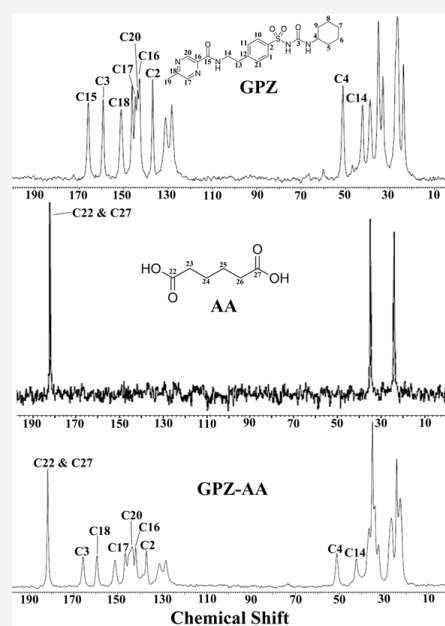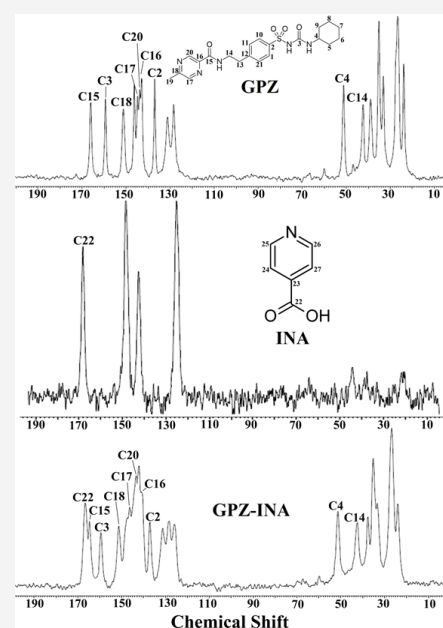

Figure 11 (A)

Figure 11 (B)

Figure 11 (c)
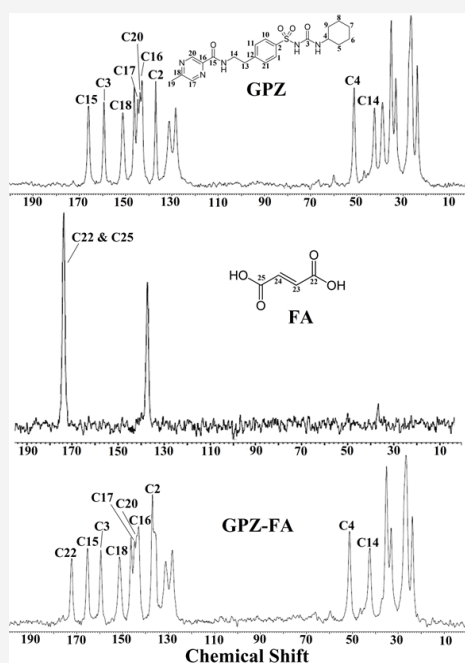
Figure 11 (D)
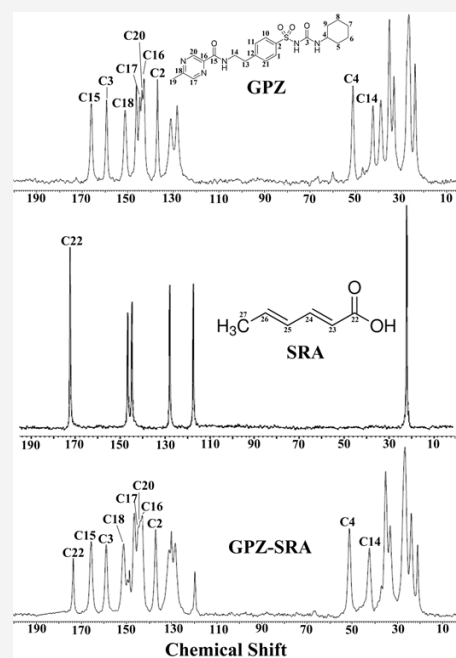
Figure 11 (E)

Figure 11: SSNMR of GPZ, coformers and its cocrystals.

The downfield shifting of C2 (attached to S1) and C4 (attached to N2) is observed in GPZ-SRA, which points towards the breaking of N1–H2⋯O1 and N2–H3⋯O1 homosynthons. Besides this, it also confirms the participation of O1 and N2–H3 in the formation

of a hydrogen bond *i.e.*, O5–H28⋯O1 (r (H⋯A): 1.825 Å) and N2–H3⋯O6 (r (H⋯A): 1.959 Å), in comparison to N2–H3⋯O1 (r (H⋯A): 2.592 Å) hydrogen bond. The formation of both heterosynthons is corroborated by upfield shifting of C22 (attached to O5 and O6).

Besides this, the upfield shifting of C3 (attached to O3), C14 (attached to N2) and downfield shift of C15 (attached to O4) suggests the breaking of N2–H3···O3 and N3–H19···O4 homosynthons (Figure 11).

## Equilibrium solubility and intrinsic dissolution rate (IDR)

The determination of equilibrium solubility and IDR of an API in the cocrystals is essential; especially in case of BCS class II drugs where bioavailability is limited by dissolution. The solubility of the coformer and the packing of API and coformer in the crystal lattice are the main contributors in the customization of the same. The cocrystals of GPZ exhibit high solubility and IDR in comparison to GPZ (Table 3). The order of their solubility (Figure 12) and IDR is GPZ-PA (6 fold) > GPZ-AA (4.5 fold) > GPZ-INA (3.7 fold) > GPZ-FA (2.3 fold) > GPZ-SRA (1.7 fold). The reason for the best equilibrium solubility and IDR of GPZ-PA may be the highest solubility of PA among all the conformers, used in the present study. GPZ-AA, the second in the solubility order can be explained on the same grounds. If the solubility of the coformers is the sole criterion for deciding the solubility of cocrystals, then GPZ-FA should be more soluble than GPZ-INA, but the observed equililibrium solubility and IDR is just reverse. This can be explained on the basis of crystal structure. It has been detailed in previous section that the strong homomeric interactions is prevailing in GPZ-FA, whereas GPZ-INA has dominating heteromeric interactions. The presence of GPZ dimer in GPZ-FA, poses the difficulties in the breaking of the crystal lattice. However, the low solubility and IDR of GPZ-SRA is only due to its low solubility (Table 3 & Figure 12).

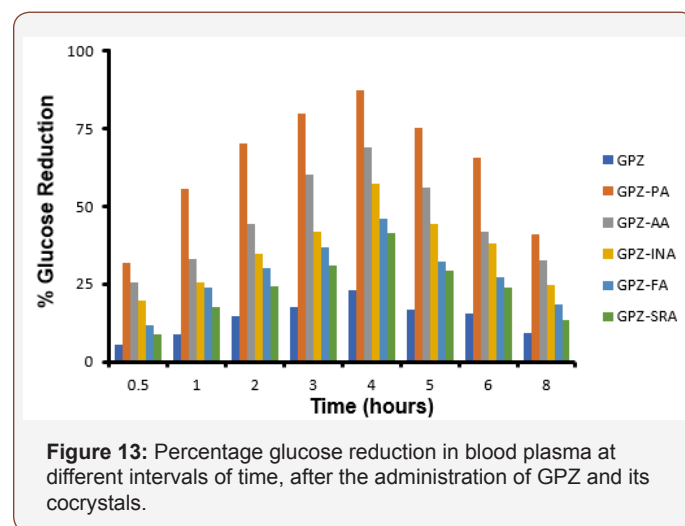**Table 3:** Equilibrium solubility and IDR of GPZ and its cocrystals[†].

	Solubility (mg/mL) ± SD	IDR (mg/min/cm²) ± SD
GPZ	0.19 ± 0.02	0.68 ± 0.02
GPZ-PA	1.15 ± 0.04	4.10 ± 0.04
GPZ-AA	0.85 ± 0.03	3.08 ± 0.03
GPZ-INA	0.70 ± 0.02	2.71 ± 0.02
GPZ-FA	0.44 ± 0.02	1.49 ± 0.03
GPZ-SRA	0.32 ± 0.03	1.18 ± 0.02

Figure 12: Equilibrium solubility of GPZ and its cocrystals (in mg/ml).
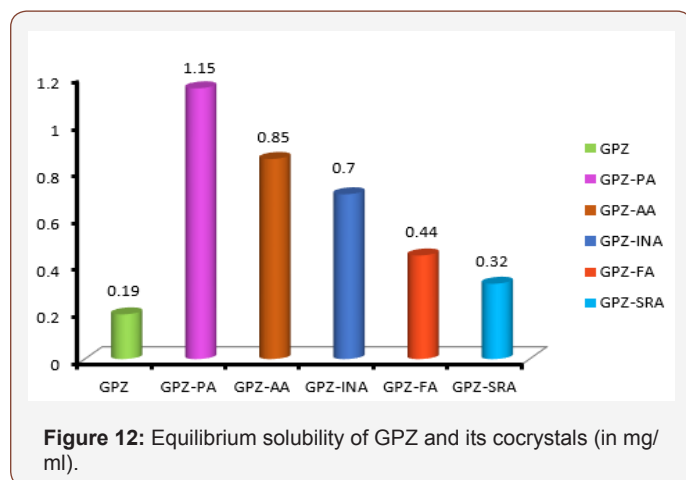
In Vivo studies

The enhancement in the solubility and IDR of an API tailors the pharmacodynamic activity and pharmacokinetic parameters.

All the cocrystals are found to be more effective in reducing blood glucose level (Figure 13) as compared to GPZ, in diabetic rats. The order of reducing blood glucose quantitatively is GPZ-PA> GPZ-AA> GPZ-INA> GPZ-FA> GPZ-SRA. C_{max} and AUC (Table 4) for all the cocrystals have been increased in comparison to GPZ, which indicates the enhanced availability of GPZ. Besides this, T_{max} is not altered significantly. All these findings point towards the increase in the extent of absorption of GPZ, without affecting the rate of absorption. All the cocrystals have better profile than GPZ and this may provide the viable alternatives for improving the regimen of diabetes by reducing the dose of GPZ (Figure 13 & Table 4).

Figure 13: Percentage glucose reduction in blood plasma at different intervals of time, after the administration of GPZ and its cocrystals.

Table 4: Percentage glucose reduction in blood plasma at different intervals of time, after the administration of GPZ and its cocrystals.

	AUC0-t ± SEM (ng/ml*min)	Cmax ± SEM (ng/ml)	Tmax(hours)
GPZ	37.14 ± 4.2	8.23 ± 2.1	4
GPZ-PA	221.16 ± 3.6	47.02 ± 1.8	4
GPZ-AA	165.24 ± 4.3	36.42 ± 3.2	4
GPZ-INA	142.03 ± 2.5	30.36 ± 2.4	4
GPZ-FA	99.54 ± 4.5	18.70 ± 2.9	4
GPZ-SRA	62.41 ± 2.6	14.01 ± 3.1	4

Conclusion

Among all the methods of improving the solubility of APIs, cocrystals are the viable means of modifying the physicochemical properties of preexisting APIs. In the present manuscript, GPZ, a BCS class II drug, was targeted for cocrystallization with the aim of improving its solubility and clinical performance. The cocrystals of GPZ were synthesized using the solvent drop grinding method which is a sustainable green approach. The existence of new crystalline phase upon grinding was identified by DSC and PXRD whereas FTIR spectral analysis imparted the information regarding hydrogen bonds among the complementary functional groups present on GPZ and coformers. The stored information in the PXRD patterns, regarding the positions of atoms in the crystal lattice were used to determine the crystal structures of the cocrystals. The supramolecular network of the cocrystals was further supported by changes in the chemical shifts shown by SSNMR. All the cocrystals exhibited high solubility, IDR and improved pharmacodynamic and

pharmacokinetic parameters as compared to GPZ. For the given data set, it has been found that solubility of the coformers and the crystal structure of the cocrystals are the main determinant of the solubility and IDR of cocrystals. The study presented herein directs the green and economical route of improving the profile of GPZ, which can potentially be developed into the formulation.

Supporting Information

DSC thermograms of physical mixture of GPZ and coformers, FTIR spectra, Rietveld plots, geometrical paramaters of crystal structure of cocrystals

Conflict of Interest

The authors declare no competing financial interest.

Acknowledgement

References

1. Bowmaker GA (2013) Solvent-assisted mechanochemistry. Chem Commun 49(4): 334-348.

2. Shearehouse WC, Waddell DC, Mack J (2009) Curr Opin Drug Discovery Dev 12, 772-783.

3. Mokhtari J, Naimi-Jamal MR, Hamzeali H, Dekamin MG, Kaupp G (2009) ChemSusChem 2(3): 248-254.

4. Strobridge FC, Judaš N, Friščić T (2010) A stepwise mechanism and the role of water in the liquid-assisted grinding synthesis of metal–organic materials. Cryst Eng Comm 12(8): 2409-2418.

5. Braga D, Giaffreda SL, Grepioni F, Pettersen A, Maini L, et al. (2006) Mechanochemical preparation of molecular and supramolecular organometallic materials and coordination networks. Dalton Trans 10: 1249-1263.

6. Braga D, Grepioni F (2004) Reactions between or within molecular crystals. Angew Chem Int Ed Engl 43(31): 4002-4011.

7. Pichon A, James SL (2008) An array-based study of reactivity under solvent-free mechanochemical conditions—insights and trends. CrystEngComm 10(12): 1839-1847.

8. Schultheiss N, Lorimer K, Wolfe S (2010) Attempted construction of minoxidil: carboxylic acid cocrystals; 7 salts and 1 cocrystal resulted. Desper J CrystEngComm 12(3): 742-749.

9. Friščić T, Trask AV, Jones W, Motherwell WD (2006) Angew Chem 118: 7708-7712.

10. Friscic T, Jones W (2009) Recent Advances in Understanding the Mechanism of Cocrystal Formation via Grinding. Cryst Growth Des 9(3): 1621-1637.

11. Nguyen KL, Friščić T, Day GM, Gladden LF, Jones W (2007) Terahertz time-domain spectroscopy and the quantitative monitoring of mechanochemical cocrystal formation. Nat mat 6(3): 206-209.

12. Karki S, Friščić T, Jones W (2009) Control and interconversion of cocrystal stoichiometry in grinding: stepwise mechanism for the formation of a hydrogen-bonded cocrystal. Cryst Eng Comm 11(3): 470-481.

13. Bowmaker GA, Chaichit N, Pakawatchai C, Skelton BW, White AH (2008) Solvent-assisted mechanochemical synthesis of metal complexes. Dalton Trans 22: 2926-2928.

14. James SL, Adams CJ, Bolm C, Braga D, Collier P, et al. (2012) Mechanochemistry: opportunities for new and cleaner synthesis. Chem Soc Rev 41(1): 413-447.

15. Patel VP, Patel NM (2009) Evaluation of Some Methods for Preparing Glipizide-βCyclodextrin

Inclusion Complexes. Iranian Journal of Pharmaceutical Sciences 5(4): 191-198.

16. Patel D, Chaudhary P, Mohan S, Khatri H (2012) e-Journal of Science & Technology 7(4).

17. Shukla M, Rathore P, Jain A, Nayak S (2010) Enhanced solubility study of glipizide using different solubilization Techniques. Int J Pharm Pharm Sci 2: 46-48.

18. Thakral S, Madan AK (2008) Urea co-inclusion compounds of glipizide for the improvement of dissolution profile. J of Incl Pheno and Macro Chem 60: 203-209.

19. Higuchi T, Connors KA (1965) Solid Dispersion Incorporated Microcapsules: Predictive Tools for Improve the Half Life and Dissolution Rate of Pioglitazone Hydrochloride. Adv Anal Chem Instrum 4: 117-212.

20. Zafar M, Naqvi SN, Ahmed M, Kaimkhani ZA (2009) Altered Kidney Morphology and Enzymes

in Streptozotocin Induced Diabetic Rats. Int J Morphol 27(3): 783-790.

21. Babu RP, Vanishree S, Sujatha S, Kishore KK (2012) Int J of Pharm and Pharm Sci 4: 133-138.

22. Trinder PJ (1969) Determination of blood glucose using an oxidase-peroxidase system with a non-carcinogenic chromogen. J Clin Pathol 22: 158-161.

23. Zhang Y, Huo M, Zhou J, Xie S (2010) PKSolver: An add-in program for pharmacokinetic and pharmacodynamic data analysis in Microsoft Excel. Comp Methods and Prog in Biomed 99(3): 306-314.

24. Newman AW, Byrn SR (2003) Solid-state analysis of the active pharmaceutical ingredient in drug products. Drug Discov Today 8(19): 898-905.

25. Burley JC (2005) Act Crystall Sec B: Struc Sci 61: 710-716.

26. Samie A, Desiraju GR, Banik M (2017) Salts and Cocrystals of the Antidiabetic Drugs Gliclazide, Tolbutamide, and Glipizide: Solubility Enhancements through Drug–Coformer Interactions. Cryst Growth Des 17: 2406-2417.